Soft-Switching Hybrid FSO/RF Links using Short-length Raptor codes: Design and Implementation

Wenzhe Zhang, Steve Hranilovic, *Senior Member, IEEE*, and Ce Shi

***Abstract*—Free-space optical (FSO) links offer gigabit per second data rates and low system complexity, but suffer from atmospheric loss due to fog and scintillation. Radio-frequency (RF) links have lower data rates, but are relatively insensitive to weather. Hybrid FSO/RF links combine the advantages of both links. Currently, selection or "hard-switching" is performed between FSO or RF links depending on feedback from the receiver. This technique is inefficient since only one medium is used at a time. In this paper, we develop a "soft-switching" scheme for hybrid FSO/RF links using short-length Raptor codes. Raptor encoded packets are sent simultaneously on both links and the code adapts to the conditions on either link with very limited feedback. A set of short-length Raptor codes ($k = 16$ to 1024) are presented which are amenable to high-speed implementation. A practical Raptor encoder and decoder are implemented in an FPGA and shown to support a 714 Mbps data rate with a 97 mW power consumption and 26360 gate circuit scale. The performance of the switching algorithms is simulated in a realistic channel model based on climate data. For a 1 Gbps FSO link combined with a 96 Mbps WiMAX RF link, an average rate of over 472 Mbps is achieved using the implemented Raptor code while hard-switching techniques achieved 112 Mbps on average.**

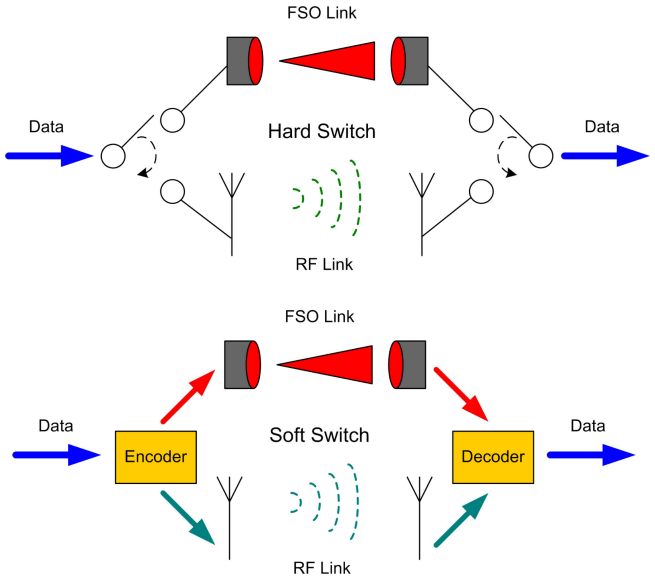

Fig. 1. Hard- and soft-switching configurations for Hybrid FSO/RF links.

I. Introduction

HYBRID free-space optical/radio-frequency (FSO/RF) links have been considered as a competitive solution for high-speed, point-to-point, wireless communications [1], [2]. They combine the advantages of the two links by inheriting the high data rate of FSO links and the reliability of RF links. Products for different data rates from 10 Mbps to multiple Gbps are currently available [3]. Hybrid FSO/RF links have also been considered for mobile applications such as robot remote control in complex environments [4], [5].

Due to their very different carrier frequencies, FSO and RF channels have distinct channel impairments. The short wavelengths used in FSO links are severely affected by scattering due to fog and atmospheric scintillation while RF links are particularly sensitive to rain scatter. Using both links in a system to overcome these unique channel impairments can result in a gain in reliability or rate.

Manuscript received 16 Januray 2009, revised 11 May 2009. This work was presented in part at the IEEE International Conference on Communications, Dresden, Germany, June 2009.

The authors are with the Department of Electrical and Computer Engineering, McMaster University, Hamilton, Ontario, Canada L8S 4K1 (e-mail: hranilovic@mcmaster.ca).

Digital Object Identifier 10.1109/JSAC.2009.0912xx.

Figure 1 presents two possible configurations for a hybrid FSO/RF link. In the hard-switching configuration, the transmitter and receiver jointly select either the FSO or RF channel for data transmission. The high-data rate FSO link is selected only if channel conditions permit reliable communications, otherwise all data are sent over the RF channel [6]. Notice that the transmitter and receiver must be co-ordinated via feedback to select the correct channel for transmission. A key disadvantage of hard-switching is that at any time one link is sitting idle. In practice, scintillation or loss in the sensitive FSO channel will cause it to be selected rarely. Once the RF link is selected, the channel capacity of FSO link is wasted.

An idea to overcome the hard-switching disadvantage is to co-ordinate data transmission in both links using channel coding, as in Fig. 1. In [7], data are encoded by a single LDPC code with a portion of the codeword split to FSO and RF links and the rate is adjusted via puncturing according to instantaneous channel conditions. Although this technique improves over hard-switching, channel conditions must be known at transmitter and receiver and complex soft decoding is required which is difficult at FSO data rates. Raptor codes have also been recently considered for hybrid FSO/RF links [8], [9]. These codes do not require channel knowledge at the transmitter and are able to adapt their rate to channel

conditions with only a single bit feedback per message. In [9], a bit-wise Raptor coding scheme is considered in which bits transmitted on FSO and RF links are random linear combinations of message bits. A well-known code is employed [8], and it is assumed that the transmitter and receiver have the interconnection information for each bit. Additionally, soft iterative detection is required at the receiver and the impact of varying atmospheric conditions is not considered.

In this work, a practical soft-switching hybrid FSO/RF system is designed and implemented using short-length Raptor codes. The advantage of using Raptor codes is that the encoder does not require channel information and the code automatically adapts the rate between RF and FSO links depending on weather conditions. This is unlike earlier work using LDPC codes, where extensive feedback is required from receiver to transmitter to adapt and synchronize code selection at both ends of the link. This work also differs significantly from recent results which apply bit-wise Raptor coding for soft-switching. We consider hard-decision, packet transmission on both FSO and RF channels due to its simplicity, practicality and wide spread use. Novel degree distributions for short-length Raptor codes are designed to permit implementation at the high data rates of FSO links. In addition, the overhead inherent in sending the interconnection information of each packet is considered explicitly rather than assuming that receiver and transmitter have synchronized random generators. Finally, simulation results on a realistic channel model using climatic data from three Canadian cities are presented to demonstrate the improvement in rate over hard-switching systems.

In Sec. II, a channel model for the hybrid FSO/RF link is presented. In Sec. III, a novel set of short-length ($k = 16$ to 1024) Raptor codes are designed to support the high rates of hybrid FSO/RF channels. The algorithm and architecture of the Raptor encoder and decoder are then discussed in Sec. IV. Simulation results on a realistic hybrid channel are given in Sec. V and the paper concludes in Sec. VI.

II. Hybrid FSO/RF Channel Model

For the point-to-point hybrid FSO/RF system in Fig. 1, the channel model is a combination of two individual line-of-sight (LOS) FSO and RF channels.

A. FSO Channel Model

In FSO systems, data are transmitted by modulating the instantaneous intensity of a laser source and detecting the received intensity with a photodiode. Define $\mathcal{X}$, $\mathcal{Y}$ as the optical intensity transmitted signal and received signal respectively. A conventional channel model is

$$\mathcal{Y} = hR\mathcal{X} + n \tag{1}$$

where h is channel gain and R is receiver responsivity [10]. A widely used optical intensity modulation scheme is on-off keying (OOK) in which $\mathcal{X} \in \{0, 2P_{\mathrm{FSO}}\}$ is selected equally likely, where P_{FSO} is the average transmitted power. In this work, it is assumed that OOK is used for the FSO links. The noise, n, is due to circuit noise as well as high-intensity background illumination and is conventionally modelled as being zero mean additive white Gaussian noise [10].

The atmospheric effects of the FSO channel include loss and scintillation. In this paper, the channel gain h is factored as [11],

$$h = h_l h_s h_g \tag{2}$$

where h_l, h_s and h_g denote the attenuation due to atmospheric loss, scintillation and geometric loss respectively. Both h_l and h_s are time-variant, however, at very different time scales. The atmospheric loss h_l varies on the order of hours while scintillation varies on the order of 1–100 ms [12]. This is in marked contrast to bit intervals which are typically 1 ns or less.

Atmospheric loss occurs due to scattering and absorption and can be modelled by the Beers-Lambert law [13],

$$h_l = e^{-\sigma z} \tag{3}$$

where σ is attenuation coefficient and z is propagation distance. The appropriate model for σ varies depending on the wavelength and weather condition. For clear and foggy weather conditions, the attenuation coefficient is linked to visibility data through Kim's model [14],

$$\sigma_{\mathrm{no-precip}} = \frac{3.91}{V}\left(\frac{\lambda}{550}\right)^{-q} \tag{4}$$

where V is visibility in km, λ is wavelength in nm and q is a parameter related to the size distribution of particles and the visibility. This model is accurate for a narrow wavelength range suitable for FSO communications [14]. In the case of precipitation, the loss is relatively wavelength insensitive. For rain, an accepted empirical model from [15] is,

$$\sigma_{\mathrm{rain}} = \frac{2.9}{V}. \tag{5}$$

For snow, the attenuation can be more severe due to a much larger droplet size. For a fair comparison with rain, following [16], we select σ_{snow} as,

$$\sigma_{\mathrm{snow}} = 20\sigma_{\mathrm{rain}}. \tag{6}$$

Atmospheric scintillation arises due to random changes in the refractive index of air along the transmission path. In every fading interval, an independent gain, h_s, is selected according to the Gamma-Gamma distribution [17],

$$\Pr(h_s) = \frac{2(\alpha\beta)^{(\alpha+\beta)/2}}{\Gamma(\alpha)\Gamma(\beta)}(h_s)^{\frac{(\alpha+\beta)}{2}-1}K_{\alpha-\beta}(2\sqrt{\alpha\beta h_s}) \tag{7}$$

where $K_{\alpha-\beta}(\cdot)$ is the modified Bessel function of the second kind and $1/\alpha$, $1/\beta$ are variances of large and small scale eddies respectively [17]. These two variances are related to the Rytov variance,

$$\sigma_R^2 = 1.23\left(\frac{2\pi}{\lambda}\right)^{7/6} C_n^2\ z^{11/6} \tag{8}$$

where C_n^2 is the refractive-index structure parameter through well-known expressions [17, pp.335-336]. The structure parameter, C_n^2, is the main parameter of the Gamma-Gamma distribution and represents the atmospheric turbulence level. Table I presents values for C_n^2 for a variety of weather

TABLE I
C_n^2 FOR DIFFERENT WEATHER CONDITIONS

Weather Condition	$C_n^2 \times 10^{-14}$ ($\mathrm{m}^{-2/3}$)	V (km)
Clear	2	> 10
Light Haze	1.8	4–10
Haze	1.5	2–4
Thin fog	1	1–2
Light fog	0.5	< 1

conditions used in this work [13], [18], [19]. Notice that turbulence is more severe in clear conditions than in foggy, high loss, conditions.

Geometric loss arises due to divergence of the transmitted beam and increases with propagation distance. For a fixed point-to-point link, assuming perfect alignment between transmitter and receiver exists and Gaussian beam profiles, the geometric loss can be approximated as,

$$h_g = \left[\mathrm{erf}\left(\frac{\sqrt{\pi}a}{\sqrt{2}w_z}\right)\right]^2, \quad w_z \approx z \cdot \phi \tag{9}$$

where w_z is the beam width at propagation distance z, $2a$ is the aperture diameter and ϕ is the divergence angle of beam [11]. The geometric loss h_g is a fixed loss for a given FSO link independent of weather conditions.

B. RF Channel Model

An IEEE 802.16 WiMAX point-to-point link RF link operating at 5.8 GHz with 64-QAM modulation is considered as a complementary link to the FSO channel [20], [21]. Commercial point-to-point WiMAX RF links achieve several km transmission distance at rates of tens to hundreds of Mbps [20], [22]. Other experimental demonstrations have shown WiMAX systems with ranges 7–50 km [20], [23].

The 5.8 GHz band is relatively insensitive to deep rain fades [24]. In addition, the requirement of an unobstructed LOS for FSO implies that multipath fading of the directive point-to-point RF link will be small. Additionally, many diversity techniques exist to mitigate the impact of fading in the RF channel. In most commercial systems, sufficient fade margin on the order of 10-15 dB, is added to the link budget to ensure highly reliable operation [35]. As a result, in this work the RF channel is modelled as a fading-free, additive white Gaussian noise (AWGN) channel. This is an optimistic model for the RF channel, however, due to the short ranges considered (< 2 km) and available diversity techniques the reliability of the RF link is many times better than commercial FSO links. As a result, the overall system reliability is limited by the FSO link and not the backup RF link.

Define the RF transmitted power as P_{RF} and the channel power gain, G_{RF}, using the Friis transmission equation as,

$$G_{\mathrm{RF}} = G_{\mathrm{tx}} G_d G_{\mathrm{rx}} \tag{10}$$

where G_{tx}, G_{rx} are the antenna gains of the transmitter and receiver with respect to an isotropic antenna and G_d is the directive gain of isotropic antenna [25]. Highly directive RF antennas are available for the WiMAX standard with G_{tx} and G_{rx} in a range 10 dBi to 30 dBi [26].

C. Impact of Practical Limitations on Channel Model

Due to the high line rates of FSO systems, the practical limitations of the transmitter and receiver must be considered in channel modelling. In a vast majority of existing commercial and experimental FSO systems, groups of transmitted bits are organized into packets for transmission over the channel. At the receiver, each bit in the packet undergoes hard-detection followed by error detection. Advanced error correction codes are typically not applied to keep cost and complexity low.

In the remainder of this work, packets of ℓ bits are transmitted over FSO and RF channels at their respective data rates. The channel models in Sec. II-A and II-B are applied to every bit transmitted on the channels and hard detection is considered at the receivers to keep hardware complexity low. In order to ensure reliable communications, a cyclic redundancy check (CRC) code is applied to each packet to detect any errors. High-speed 32-bit CRC encoders/decoders complying with the IEEE 802.3 standard exist with negligibly small probability of undetected error [27]. As a result, any packets corrupted in the RF or FSO channel are discarded by the receiver. The end-to-end channel for both the FSO and RF links is a packet erasure channel with erasure probabilities θ_{FSO} and θ_{RF} respectively, as shown in Fig. 2. Note that θ_{FSO} is highly sensitive to the particular weather condition.

III. DESIGN OF SHORT-LENGTH RAPTOR CODES

A packet-level coding technique using Raptor codes is developed here to achieve efficient soft-switching in hybrid FSO/RF links. A sequence of Raptor-encoded outputs are generated from the message packets, as in Fig. 2, and sent over FSO and RF links simultaneously. Notice that there is no co-ordination between RF and FSO links and packets are sent either on RF or FSO channels at their respective transmission rates. The receiver collects packets that were not discarded by the equivalent FSO/RF erasure channels and the entire message is decoded when sufficient packets are received. It is assumed that the transmitter continues sending encoded packets for a given message until a 1-bit feedback is received to proceed to the next message. In this section, a set of short-length $k = 16$–1024 Raptor codes are presented which adapt the rate among the FSO and RF channels according to the channel conditions using limited feedback.

A. Background on Raptor codes

Raptor codes are random bipartite graph codes in which every encoded packet is a linear combination of a random number of message packets [8]. A message consists of k packets each of length ℓ bits (Fig. 2). The *degree* of an encoded packet is the number of message packets combined, and is chosen randomly and independently for each encoded packet. Raptor codes consist of an LT code [28] and a pre-coding low-density parity-check (LDPC) code. This LDPC code enlarges the effective number of message packets from k to $\hat{k}$ [8].

Define m as the number of received packets necessary for successful decoding of a k-packet message. Since the Raptor encoder generates packets in a random fashion, so too m is

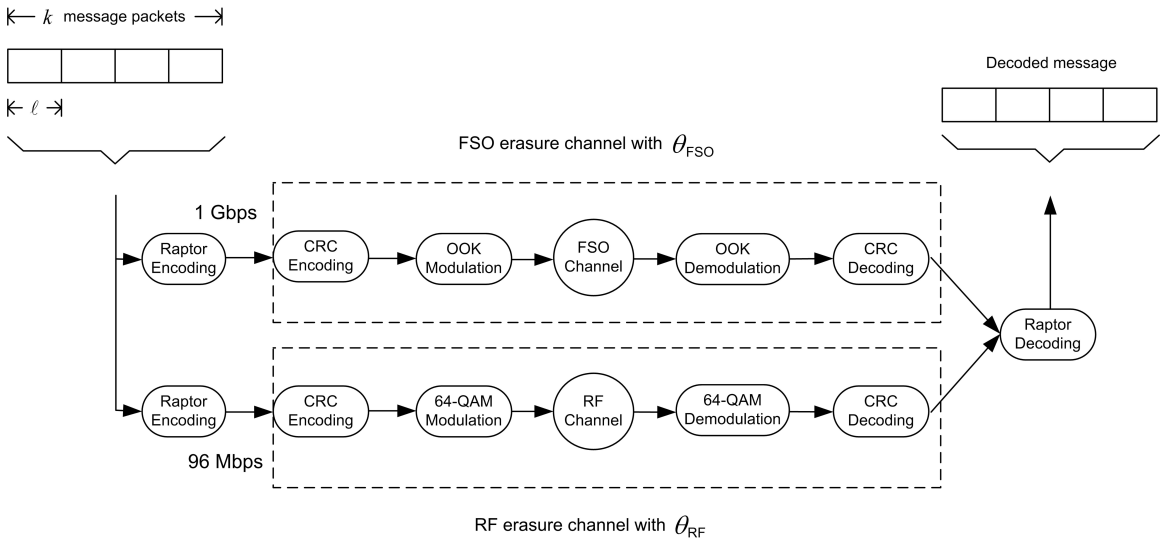

Fig. 2. Soft-switching hybrid FSO/RF link using packet-level Raptor codes.

random. Define the expected overhead of a Raptor code, ε_m, as

$$\langle m \rangle = (1 + \varepsilon_m)k \tag{11}$$

where $\langle \cdot \rangle$ denotes expectation. The statistical overhead, ε_m, is inherent to the Raptor code and independent of the channel.

The *degree distribution* polynomial of a Raptor code is defined as $\Omega(x) = \Sigma_{i=1}^{\hat{k}} \Omega_i x^i$, where the x^i term represents a degree i, and Ω_i is the probability mass of degree i. Raptor codes are decoded via a simplified belief propagation (BP) algorithm. The algorithm starts from a degree one packet and uses it to decode packets of larger degree. Decoded packets are subtracted from all larger degree packets which involve it. All received packets are stored in a buffer and the decoding process continues searching and subtracting until the k message packets are recovered. Section IV presents efficient hardware implementation of a Raptor encoder and decoder.

The decoding complexity of a Raptor code has been shown to be $O(k \log 1/\eta)$ on average, where $\eta > 0$ is a design code overhead set typically at a couple percent [8]. Selecting a short k is advantageous to reduce complexity in decoding. However, in earlier Raptor code designs [8], an apparent trend was that reducing k resulted in an increase in ε_m, i.e., a reduction in rate. A $k = 9500$ Raptor code has also been widely used [29], however, for the Gbps rates considered for FSO channels decoding such a code is complex.

B. Pre-Coding LDPC

The LDPC code is selected to be systematic and each $\hat{k} - k$ redundant packet has degree D. The D message packets connected to each check node are chosen uniformly and independently. To each message, $\hat{k} - k = 0.02k$ redundant LDPC packets are added for $k = 64$ to 1024, and a single packet is added for $k = 16, 32$. Table II lists the selected degree D, of each redundant packet for different k. Initially D is set to $\log_2 k$ for a given degree distribution and increased to reduce ε_m after simulation. The degree distribution is then optimized, following Sec. III-C, and the process repeated until the overhead cannot be reduced further. Note, this heuristic optimization is typical in the design of such codes, and different pre-coding LDPC codes can achieve similar performance [8].

TABLE II
DEGREE OF LDPC PRE-CODE AND c FOR DIFFERENT k

k	16	32	64	128	256	512	1024
D	9	16	19	27	30	33	44
c	0.04	0.05	0.05	0.07	0.08	0.08	0.09

C. Design of Degree Distribution

The *input ripple* is defined as the set of message packets decoded up to a particular step [8]. A good code maximizes the input ripple throughout the decoding process. Reference [8] gives a heuristic proposal: for $x \in [0, 1 - \delta]$, where δ is the fraction of message packets not decoded, keep the ripple size $\geq c\sqrt{(1-x)\hat{k}}$, where c is a small constant. Using this proposal, it was shown that $\Omega(x)$ should satisfy

$$\Omega^{'}(x) \geq \frac{-\ln\left(1 - x - c\sqrt{\frac{1-x}{\hat{k}}}\right)}{1+\eta}, x \in [0, 1-\delta] \tag{12}$$

where $\Omega^{'}(x)$ is the derivative of $\Omega(x)$ [8].

In this work, we proceed as in [8], and for a given degree distribution, (12) is verified by discretizing the interval $[0, 1 - \delta]$ in steps of 0.001. Since there are many degree distributions satisfying (12), we base our design of $\Omega(x)$ for short k on the degree distribution for a long Raptor code of $k = 64536$ [8]

$$\Omega^*(x) = 0.007969x + 0.49357x^2 + 0.16622x^3 + 0.072646x^4 + 0.082558x^5 + 0.056058x^8 + 0.037229x^9 + 0.05559x^{19} + 0.025023x^{65} + 0.003135x^{66}. \tag{13}$$

A heuristic technique must be applied to find $\Omega(x)$ for $k = 16$ to 1024 since no analytical design procedures exist. A typical value $\eta = 0.05$ is selected as in [8]. Following [8], to verify (12), $c < \delta\sqrt{\hat{k}}$ and $\delta = 0.01$. Care must be taken in selecting the value of c to ensure (12) is satisfied. Table II

TABLE III
DESIGN RESULTS FOR $\Omega(x)$

k	16	32	64	128	256	512	1024
Ω_1	0.18	0.11	0.1	0.06	0.04	0.025	0.015
Ω_2	0.52	0.5	0.5	0.495	0.495	0.495	0.495
Ω_3	0.1	0.13	0.11	0.16	0.167	0.167	0.167
Ω_4	0.2		0.08	0.08	0.08	0.082	0.082
Ω_5		0.26	0.042	0.05	0.07	0.071	0.071
Ω_8				0.037	0.039	0.05	0.049
Ω_9			0.045	0.02	0.025	0.044	0.048
Ω_{11}			0.06				
Ω_{13}			0.063				
Ω_{16}				0.04			
Ω_{19}				0.058	0.035	0.043	0.05
Ω_{25}					0.049		
Ω_{66}						0.023	0.023

lists the values of c chosen after extensive simulation. To find an $\Omega(x)$ with good performance, $\Omega^*(x)$ is modified stepwise until (12) is satisfied.

Step 1: Truncate the large degree items in $\Omega^*(x)$ larger than $k/4$. For example, x^5 to x^{66} terms are removed for $k = 16$. From [8], it is not necessary that $\Omega(x)$ have packets of every degree. Qualitatively, adding large degree packets also increases d_{avg} significantly.

Step 2: Add x^{11}, x^{13}, x^{16} and x^{25} to $\Omega(x)$ for $k = 64$, 128 and 256. Packets of large degree are important to ensure that all message packets are covered. However, for the small k considered, the large degrees in $\Omega^*(x)$ are excessive. Therefore, moderate degree terms are added as a trade-off between x^9 and x^{66} terms.

Step 3: Increase probabilities Ω_i for small degrees significantly, especially for degree one. For example, for $k = 16$, increase Ω_1 from 0.007969 to 0.18. After $\Omega^*(x)$ is truncated in step 1, Ω_i of large degree terms is shifted to smaller degrees. If Ω_1 increases, more packets of degree one are sent in early stages of decoding. This shifting also reduces d_{avg}, the average decoding cost. Increasing Ω_1 too much, however, can stall decoding since the encoded packets may not cover enough message packets. Therefore, Ω_1 is increased and checked via simulation to ensure good operation.

After the heuristic steps above, an initial $\Omega(x)$ is obtained for each k. However, the initial design is often not robust and has large d_{avg} and ε_m. To improve performance, for each k and choice of $\Omega(x)$ many simulations are performed to estimate the distribution of m. Qualitatively, if ε_m is large from simulation, then more probability is shifted from large degree to small degree. This search procedure continues in this fashion until ε_m cannot be reduced any further. Table III presents the resulting degree distributions.

D. Results of Code Design

The performance of the codes defined in Tbl. III is plotted in Fig. 3. Notice that ε_m decreases with an increasing k. When $k = 1024$, ε_m decreases to 0.126. However, d_{avg} increases with k. For $k = 1024$, $d_{\text{avg}} = 6.32$, which can be considered as a moderate decoding cost. Compared to $k = 64536$ code using $\Omega^*(x)$ from (13) [8], coding overhead, ε_m, for $k = 1024$ is 8% larger than for $k = 64536$, however, d_{avg} is approximately 37% less. This is a significant trade-off between a slight increase in coding overhead ε_m and a large decrease in decoding complexity, i.e., d_{avg}.

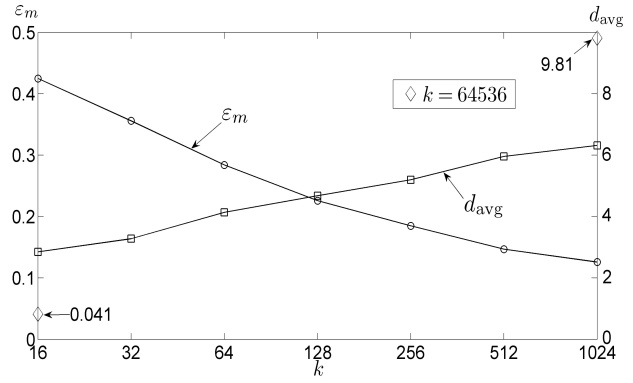

Fig. 3. Overhead, ε_m, and average degree, d_{avg}, of designed Raptor codes. Note that points indicated by '$\diamond$' indicate performance using $\Omega^*(x)$ (13).

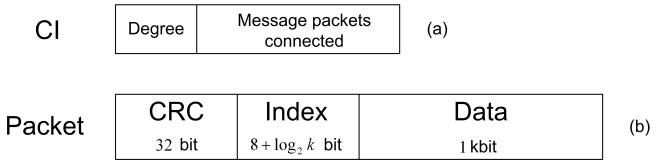

Fig. 4. Connection information (CI) and packet structure.

IV. IMPLEMENTATION OF RAPTOR ENCODER AND DECODER

The design of short-length Raptor codes with lower complexity enables the implementation of high-rate decoders. This section presents the design procedure and performance of an implemented Raptor encoder/decoder appropriate for hybrid FSO/RF links.

A. Algorithm of Raptor Encoder

Every encoded Raptor packet must carry information about how it is interconnected to the message packets. In this work, define the *connection information*, (CI), of an encoded packet as its degree and the list of all message packets used to construct it, as shown in Fig. 4(a). Notice that the number of bits required to encode the CI for a particular packet can vary significantly.

In order to obtain a fixed-size transmitted packet, a finite set of CI's are stored at both transmitter and receiver in a table termed the *CI table* (CIT). Thus, only the index into this table need to be transmitted with each packet. For $k = 16$–1024, the size of index is $8 + \log_2 k$ bit, less than 2% of the packet for $\ell = 1024$, as shown in Fig.4(b). In Sec. IV-F the size of the memory required for the CIT is quantified in a practical implementation.

In this work, to simplify implementation, the random generation of packet interconnections is replaced by a pre-computed CIT. This table is formed by using a pseudo-random generator to select degrees according to $\Omega(x)$. In addition, the interconnection of the LDPC pre-coded packets are included in the entries of the CIT. In order to ensure good performance,

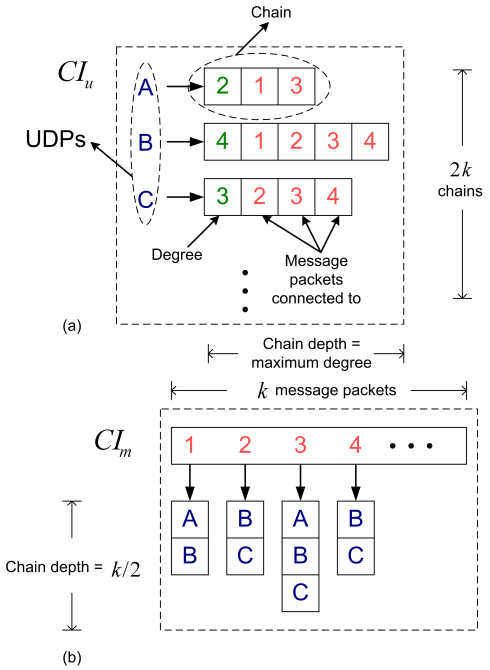

Fig. 5. Structure of chain lists (a) CI_u and (b) CI_m.

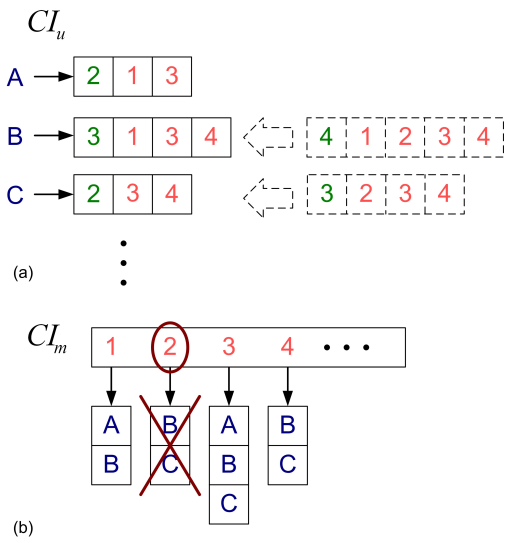

Fig. 6. Example of chain list access.

the length of the CIT must be long enough to thoroughly sample possible degree selections. After extensive simulation, the CIT table is set to contain $256 \cdot k$ elements. The same CIT is implemented at both encoder and decoder. For a given index the CI is known and the data of the indicated packets are added using a packet-length exclusive-or (XOR). Then the index is appended to the encoded data and a CRC is added. After the encoding of a packet is completed, the encoder moves to the next packet and the index in the CI is incremented.

B. Algorithm of Raptor Decoder

Define *undecoded packets* (UDP) as received packets whose degree is greater than 1. Conversely, define *decoded packets* (DP) as degree one packets which have been released in previous decoding stages. Finally, define *newly released packets* (NRP) as degree one packets which are released in the current decoding stage. Undecoded packets, decoded packets and newly released packets are stored separately. The following discussion summarizes the five steps of the modified BP algorithm.

Step 1: Input a packet, and check CRC. If pass, then translate the index to CI by lookup in the CIT.

Step 2: If the input packet is a degree one packet which has not yet been decoded, place it in the NRP memory. Otherwise, place it in the UDP memory and XOR with any previously decoded packets in the DP memory. This step may release new degree one packets, which are saved to the NRP memory, or reduce the degree of received packet.

Step 3: New released packets in the NRP memory are used to repeat Step 2 until no new degree one packets are released.

Step 4: Copy all NRP to the DP memory.

Step 5: If all k message packets are decoded in the DP memory, the decoding process stops. Otherwise, input a new packet and repeat Step 1.

C. Chain List of Raptor Decoder

To minimize the decoding time, the CI of undecoded packets must be recorded in a data structure which permits quick access. Define a *chain list* as an indexed set of lists, or *chains*, similar to a hash table with separate chaining. For example, to store the connection information for undecoded packets define a chain list CI_u in Fig. 5(a). Each UDP indexes a list containing the CI corresponding to the packet. By convention, the first entry in each chain is the degree of the packet and is set to ease implementation. Entries are made sequentially into CI_u each time a packet is added to the UDP memory. Though the degree of UDPs varies randomly, the size of the memory must be fixed. In this work, the depth of the chain list is set to the maximum degree in $\Omega(x)$. Once the degree of the UDP is reduced to one by the decoding algorithm it is moved to the NRP memory.

In order to avoid expensive searches through CI_u, another chain list CI_m is defined to hold the connection information of each message packet, as illustrated in Fig. 5(b). In CI_m, the k message packets index chains containing the set of UDPs which depend on the message packet. For example, from Fig. 5(b), UDPs A and B depend on message packet 1. Once the CI of a UDP is added to the CI_u, the index of this entry is also stored in every chain of CI_m connected to packet. For example, notice that packet A in CI_u in Fig. 5(a) is also contained in chains 1 and 3 of CI_m in Fig. 5(b).

To illustrate the operation of these chain lists, consider a case where the chain lists CI_u and CI_m are as in Fig. 5. Suppose a degree one packet is received containing message packet 2. Figure 6 illustrates the operation on the chain lists. First, CI_m is accessed indicating that UDP packets B and C depend on message packet 2. Then, chains B and C in CI_u are accessed, the degree is reduced by one and the reference to message packet 2 is removed. Finally, the chain for message packet 2 in CI_m is removed. In this way, the CI of remaining UDPs and message packets remains consistent and is easily accessed and modified.

The decoding time of Raptor codes can be divided into two

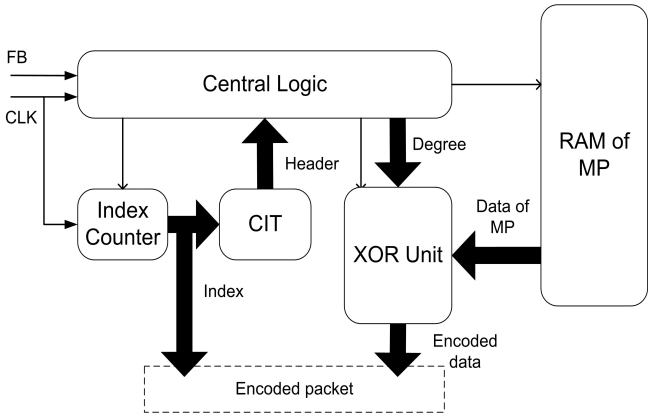

Fig. 7. Architecture of Raptor encoder (MP=message packet). Thin lines are control signals while thick lines indicate data paths. FB = feedback from decoder indicating message received.

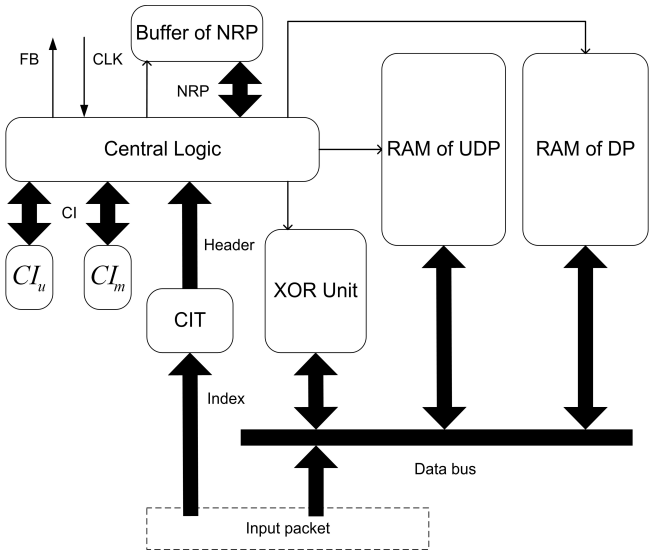

Fig. 8. Architecture of Raptor decoder. Thin lines are control signals while thick lines indicate data paths. FB = feedback from decoder indicating message decoded.

parts: the XOR operation on the data and chain list access to maintain interconnection information. Though CI_u and CI_m are accessed directly, update and deletion of chain list still costs time.

To get a rough estimate of the decoding speed for the Raptor codes designed in Sec. III, the decoding algorithm with chain lists is simulated for $k = 16$–1024 on a PC. In software, CI_u and CI_m are implemented in memory accessed by CPU. Each update of a chain list element at least contains "read", "assign value" and "write" command cycles. The PC has an AMD Athlon X2 3800+ CPU clocked at 2.0 GHz and the Dev-C++ compiler was used for all simulations. The results of the simulation for $k = 16$–1024 indicate that the estimated decoding speed varies from 1.4 Gbps to approximately 50 Mbps. Limited by the chain list access, the average decoding time of every packet increases significantly with k. When k increases, the larger d_{avg} incurs a greater number of XOR operations. Though ε_m decreases with increasing k, from the discussion of Sec.III-D, it is also clear that the decoding complexity increases significantly. Thus, for the high data rate FSO channels considered here, Gbps performance is only available from short-length Raptor codes.

To select the size of the tables containing CI_u and CI_m, extensive simulations were conducted to avoid overflow. For CI_u, it is assumed that the maximum number of undecoded packets is $2k$, as shown in Fig. 5. For CI_m the length of the depth of each chain was set to $k/2$. After more than 10^9 runs, simulations indicate that on average the CI_u is only 23% filled and the CI_m is 46% full. No errors were encountered in the simulation nor were errors encountered for tables of this size in the hardware implementation in Sec. IV-F. Although the size of CI_u and CI_m is significant, it is still acceptable for small k.

D. Architecture of Raptor Encoder

Figure 7 presents the hardware architectures of the Raptor encoder for the designed $k = 16$ code. Several modules are included under the top level encoder design. The *index counter* is a counter which records the index of current packet in the CIT. The CIT is implemented with a 64 kbit ROM in the design. The *XOR Unit* can add two packets in each clock cycle. The *degree* signal controls the the number of XOR operations required. The *Central Logic* block is a finite state machine to co-ordinate the actions of other modules during encoding.

The primary challenge in designing the encoder is that each encoded packet requires a different number of operations due to its random degree. The Central Logic unit co-ordinates data access to the message packet (MP) memory and XORs to ensure synchronous operation. The encoding process for a given message is stopped when the feedback (FB) signal is asserted and the Central Logic unit moves to the next message in the MP RAM.

E. Architecture of Raptor Decoder

From the previous discussion, accesses to chain list dominate the decoding time. For this hardware design, however, CI_u and CI_m are both implemented with registers. This means that in one CLK cycle, update or deletion of any element in a chain can be finished. This is a hardware method to implement the chain list and in fact each chain is a circuit cell. The top level scheme of Raptor decoder is shown in Fig.8. The CIT and XOR Unit modules of Raptor decoder are the same as those of the encoder. The FB output indicates when the entire message is decoded.

From Sec. IV-B, the undecoded, decoded and newly released packets are stored in separate memories. A data bus connecting these RAMs and XOR Unit is used. There are many access to RAM during the decoding process. For example, data of an undecoded packet is read first, then XORed by data of a decoded packet and written back to UDP RAM.

F. Implementation Results

The design of Raptor encoder and decoder is implemented in a Xilinx Virtex II-Pro XC2VP100 FPGA with ISE software [30], [31]. Average encoding and decoding speed of Raptor encoder are measured at maximum clock frequency at 120 MHz. Power consumption of the circuit is estimated

TABLE IV
FPGA IMPLEMENTATION RESULTS OF RAPTOR ENCODER AND DECODER $k = 16$

	Encoder	Decoder
CLK frequency (MHz)	120	120
Data bus width (bit)	64	64
Equivalent gates	8230	26360
ROM size (kbit)	64	64
Power consumption (mW)	23	97
Required data RAM (kbit)	16 (MP)	32 (UDP)+16 (DP)
Speed (bps)	1.22 G	714 M

using the Xilinx XPE power estimate tool [32]. Details of implementation result are presented in Tbl.IV.

Due to its simplicity, the speed of the encoder is faster than the decoder and thus, the Raptor decoder limits data rates of soft-switching hybrid FSO/RF systems. In this work, an FPGA hardware design achieves decoding speed as 714 Mbps with a 120 MHz clock.

Previous Raptor code implementations have been reported at several Gbps data rate on a 2.4 GHz Intel Xeon CPU, and 27 Mbps on a 206 MHz Intel StrongARM processor [8], [33]. Neither reference gives details on the code designed or its performance. However, such rates must be considered in light of the hardware complexity of such systems. In this work, comparable data rates are realized using far simpler hardware at a much lower clock frequency. This architecture offers high rate at acceptable power consumption and circuit scale for a hybrid FSO/RF link, which will be demonstrated in Sec. V. In addition, the architecture is flexible and rates should scale with improved digital hardware implementations, i.e. FPGA or ASIC. The Raptor encoder and decoder can also be integrated in a plug-in module for WiMAX systems at an affordable extra cost. Since the Raptor codes are applied at packet level, it is possible to apply this design in not only WiMAX standard, but also other wireless standards.

V. SIMULATION OF SOFT-SWITCHING HYBRID FSO/RF SYSTEM

From the channel model described in Sec.II, the data rate of FSO channel is severely affected by weather condition. During fog conditions, the intensity of optical signal is greatly attenuated, following (4). Even in clear conditions, the optical power is still impacted by scintillation according to (7). The WiMAX RF channel working at 5.8 GHz has a lower data rate but is much more stable than the FSO channel over weather conditions. In well designed point-to-point systems, the impact of fading and noise at this RF frequency are small. With a lower transmission rate, the WiMAX RF link can be recognized as a backup of the FSO link. The parameters of the FSO and RF link for simulation are presented in Tbl.V and are chosen from [18], [20], [34], [35].

After application of the CRC, the effective channel for both RF and FSO links is an erasure channel. Since Raptor codes are applied, an increase in $\theta_{\rm FSO}$ due to atmospheric conditions will cause the decoded data rate to scale down appropriately.

The simulations are based on 2007 climate data from [36]. Since only hourly data is available, it is assumed that atmospheric parameters C_n^2 and V do not change within an hour. Although atmospheric measurements at a smaller time scale have been reported [37], they consider a measurement period of hours rather than having measurements over a longer time period. The coherence time of optical scintillation is taken to be 10 ms from [12]. In every coherence interval, a channel gain h_s due to scintillation is generated according to (7). The threshold of OOK detector in the FSO receiver is fixed for each coherence interval and selected according to the average gain. Practical link distances, $z = 0.5$, 1 and 2 km are simulated.

TABLE V
PARAMETERS OF THE FSO AND RF LINK FOR SIMULATION

FSO link		
Parameter	Symbol	Value
Wavelength	λ	1550 nm
Transmission rate	$\xi_{\rm FSO}$	1 Gbps
Transmitted power	$P_{\rm FSO}$	320 mW
Receiver responsivity	R	0.5 A/W
Variance of noise	$N_{\rm FSO}$	10^{-14} A^2
Laser divergence angle	ϕ	2 mrad
Receiver diameter	$2a$	20 cm
RF link		
Parameter	Symbol	Value
Frequency	f	5.8 GHz
Transmission rate	$\xi_{\rm RF}$	96 Mbps
Transmitted power	$P_{\rm RF}$	16 mW
Bandwidth	B	20 MHz
Variance of noise	$N_{\rm RF}$	10^{-10} mW
Antenna gain of transmitter	$G_{\rm tx}$	16 dBi
Antenna gain of receiver	$G_{\rm rx}$	30.4 dBi

Simulations are also performed for climate data for three Canadian cities: Vancouver, Toronto and St. John's. These cities are located in west coast, south border and east coast of the country respectively. All of cites are located at latitudes of 49^o–43^o North. The climate of Vancouver is moderate oceanic, where most rainfall occurs in winter. Toronto has a humid continental climate, where summer is warm and rainy, and winter is cold and snowy. From an FSO communications perspective, St. John's has the most challenging climate. In a large portion of a year, it is foggy, cloudy or snowy. For example, on average St. John's experiences 126 days of fog per year [38]. St. John's is also affected by tropical storms from the Atlantic Ocean.

The hybrid FSO/RF links are simulated with hard-switching and soft-switching with the designed short-length Raptor codes with message lengths $k = 16$ and 1024. Although the $k = 16$ case is practical and less complex, it has a much higher overhead than $k = 1024$ code as presented in Fig. 3. For hard-switching, it is assumed that in each coherence interval of 10 ms, the hard-switching system can detect the instantaneous received optical power. If the received power is 3 dB over the threshold to get 10^{-9} BER, the FSO link is selected, otherwise, the RF link is selected [6].

Average daily data rates are simulated for three link ranges in the three target cities using a variety of hard- and soft-switching techniques. Figures 9, 10 and 11 present the daily average data rates for St. John's for a variety of ranges while Tbl.VI presents results for all cities. From the three figures it is apparent that the data rates vary depending on the time of year. Typically, higher rates are available in summer months while

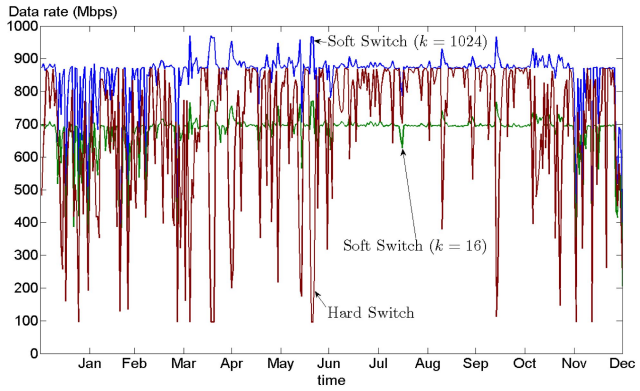

Fig. 9. Daily average data rates in St. John's, range $z = 0.5$ km.

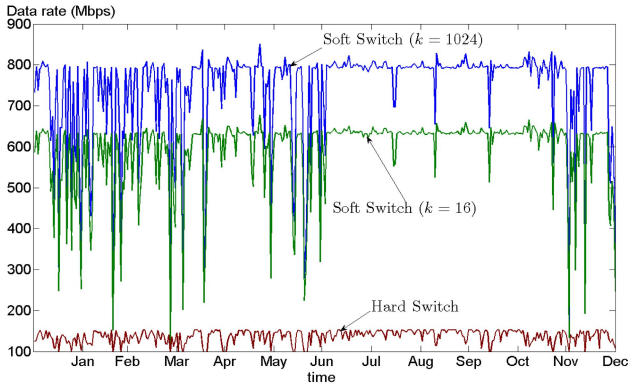

Fig. 10. Daily average data rates in St. John's, range $z = 1$ km.

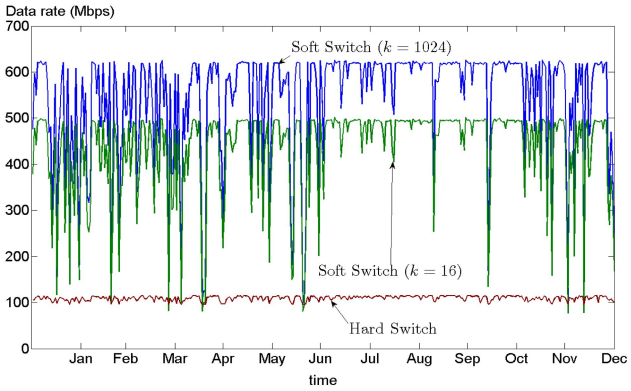

Fig. 11. Daily average data rates in St. John's, range $z = 2$ km.

TABLE VI
SIMULATION RESULT OF AVERAGE DAILY DATA RATES

Vancouver (Mbps)			
	$z = 0.5$ km	$z = 1$ km	$z = 2$ km
Soft switch ($k = 1024$)	869.3	788.5	610.9
Soft switch ($k = 16$)	692.8	628.4	487.6
Hard switch	839.4	147.6	113.0
Toronto (Mbps)			
	$z = 0.5$ km	$z = 1$ km	$z = 2$ km
Soft switch ($k = 1024$)	862.3	774.2	590.9
Soft switch ($k = 16$)	687.0	617.6	472.0
Hard switch	803.4	145.8	112.4
St.John's (Mbps)			
	$z = 0.5$ km	$z = 1$ km	$z = 2$ km
Soft switch ($k = 1024$)	846.8	737.2	538.9
Soft switch ($k = 16$)	674.7	587.9	430.7
Hard switch	689.8	136.6	109.4

low rates occur in winter months due to snow, rain and fog conditions. The temperate climate of Vancouver gives rise to less variation in rates than Toronto or St. John's. In all cases, for $z \geq 1$ km the soft-switching Raptor codes outperform hard-switching.

However, from Fig. 9 and Tbl. VI, when $z = 0.5$ km the optical power is high enough to achieve the required BER on the FSO system and little hard-switching occurs. In this case, the lower overhead of hard-switching gives better performance. Thus, when the received optical power is high enough, hard-switching is a good option which has been considered in many previous contexts [2], [6] . In this case, due to the overhead of the Raptor code ε_m, CRC and index, the data rates of soft-switching $k = 16$ Raptor codes is lower. However, the lower overhead of $k = 1024$ Raptor codes does realize a small gain in average rate.

For longer range links, $z = 1$ and 2 km, the optical power is reduced by loss and scintillation significantly. Hard-switching turns to the backup RF link frequently, wasting any available FSO data rate, and causes a total data rate decrease. Soft-switching with Raptor codes achieves much higher data rates for these cases. The $k = 16$ Raptor code improves data rate from the 100 Mbps level of hard-switching to 400 Mbps. This data rate is easily supported by the 714 Mbps rate of the implemented decoder in Sec. IV at decoder. Although an implementation for $k = 1024$ is not presented here, it is an interesting future direction due to the higher supported rates.

Figure 12 shows the distribution of the hourly data rate for St. John's for the three switching schemes at link distance of 1 km. Notice that in the case of hard-switching, the distributions are dominated two large peaks indicating that either RF or FSO links are selected. In contrast, the soft-switching hybrid FSO/RF channels have larger average rates and are able to exploit both channels simultaneously. The soft-switching schemes have a larger variance in data rate than the hard-switching due to the ability of the Raptor codes to adapt to the variable channel conditions. This in turn may incur some additional complexity due to the adaptive rate of the channel which is compensated by the larger available average rates.

Define reliability of the hybrid system as the probability that the data rate is greater than a given value R_0 as,

$$\text{Reliability} = \Pr(\text{data rate} \geq R_0) \times 100\% \qquad (14)$$

The R_0 corresponding to 99%, 99.9% and 99.99% reliability of the year are presented respectively in Tbl. VII. For hard-switching, high reliability $\geq 99\%$ requires that the RF link is selected often and the data rate is close to RF transmission rate 96 Mbps. The rates for a given reliability level are lower with soft-switching than hard-switching due to the overhead of the code. However, this small loss in reliability is compensated by the a large increase of average data rate. Thus, at longer ranges, soft-switching gives a trade-off of slightly lower reliability for a larger average data rate. The key advantage of soft-switching is that loss and scintillation need

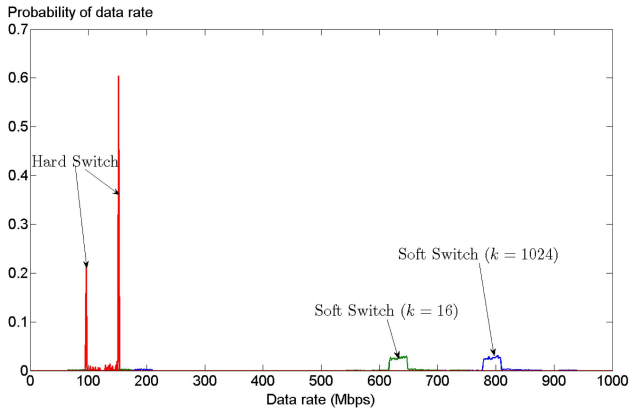

Fig. 12. Distribution of hourly data rate for soft-switching hybrid FSO/RF link in St. John's $z = 1$ km

TABLE VII
SIMULATION OF DATA RATE, R_0, FOR DIFFERENT RELIABILITIES IN ST. JOHN'S ($z = 1$ KM)

(Mbps)	99%	99.9%	99.99%	Average rate
Soft switch ($k = 1024$)	90	82	81	737.2
Soft switch ($k = 16$)	73	66	64	587.9
hard-switching	96	96	96	136.6

not be considered at the transmitter directly. No matter the weather condition, soft-switching based on short-length Raptor codes can achieve a high average data rate. Soft-switching with Raptor codes avoids the disadvantage of frequent switching between FSO and RF links and is able to simultaneously use both links, improving efficiency.

VI. CONCLUSIONS

In this paper, we proposed a soft-switching scheme for hybrid FSO/RF links with packet-level Raptor codes. We design short-length Raptor codes ($k = 16$–1024) which achieve high data rate and low decoding cost. A hardware encoder and decoder for $k = 16$ are implemented in an FPGA to demonstrate the practicality of soft-switching in hybrid FSO/RF links. For the Raptor code with $k = 16$, the hardware Raptor encoder/decoder achieves a 714 Mbps data throughput. It is sufficient to support the high rate of hybrid FSO/RF link at several hundred Mbps. Also, with the 97 mW low power consumption and 26360 gates circuit scale, it is easy to add this Raptor encoder and decoder to any current systems with an affordable extra cost. To investigate the data rate in a practical environment, parameters from a 1 Gbps FSO link and a 96 Mbps WiMAX RF link are used to simulate the hybrid FSO/RF link. Simulation with 2007 climate data of three Canadian cities shows that soft-switching with $k = 16$ Raptor code achieves average data rates of at least 430 Mbps for a transmission distance $z = 2$ km compared to 109 Mbps data rate for hard-switching. Thus, soft-switching hybrid FSO/RF links based on short-length Raptor codes are both practical and efficient in co-ordinating the simultaneous use of these channels.

REFERENCES

[1] I. I. Kim and E. J. Korevaar, "Availability of Free Space Optics (FSO) and Hybrid FSO/RF Systems," *Proc. SPIE*, pp. 84–95, Nov. 2001.

[2] E. Leitgeb, M. Gebhart, U. Birnbacher, W. Kogler, and P. Schrotter, "High Availability of Hybrid Wireless Networks," *Proc. SPIE*, pp. 238–249, Sep. 2004.

[3] "System Support Solutions," http://www.systemsupportsolutions.com/models.htm. [online], last accessed: Mar. 30, 2009.

[4] J. Derenick, C. Thorne, and J. Spletzer, "Hybrid Free-Space Optics/Radio Frequency (FSO/RF) Networks for Mobile Robot Teams," "Multi-Robot Systems: From Swarms to Intelligent Automata," A. C. Schultz and L. E. Parker (eds.), Springer, Mar. 2005.

[5] S. D. Milner and C. C. Davis, "Hybrid Free Space Optical/RF Networks for Tactical Operations," *Proc. IEEE Mil. Commun. Conf.*, pp. 409–415, 2004.

[6] A. Akbulut, H. G. Ilk, and F. Ari, "Design, Availability and Reliability Analysis on an Experimental Outdoor FSO/RF Communicaiton System," *Proc. IEEE Int. Conf. Transparent Opt. Networks*, pp. 403–406, 2005.

[7] S. Vangala and H. Pishro-Nik, "Optimal Hybrid RF-Wireless Optical Communication for Maximum Efficiency and Reliability," *Proc. IEEE Annu. Conf. Inform. Sci. Syst.*, pp. 684–689, 2007.

[8] A. Shokrollahi, "Raptor codes," *IEEE Trans. Inf. Theory*, vol. 52, no. 6, pp. 2551–2567, Jun. 2006.

[9] A. AbdulHussein, A. Oka, and L. Lampe, "Rateless Coding for Hybrid Free-Space Optical and Radio-Frequency Communication," *submitted to IEEE Trans. Wireless, under review*.

[10] X. Zhu and J. M. Kahn, "Free-Space Optical Communication through Atmospheric Turbulence Channels," *IEEE Trans. Commun.*, vol. 50, no. 8, pp. 1293–1300, Aug. 2002.

[11] A. A. Farid and S. Hranilovic, "Outage Capacity Optimization for Free-Space Optical Links With Pointing Errors," *IEEE J. Lightwave Tech.*, vol. 25, no. 7, pp. 1702–1710, Jul. 2007.

[12] E. Leitgeb, M. Gebhart, and P. Fasser, "Reliability of Free Space Laser Communications-Investigations at the TU Graz," *Proc. Annu. WCA Tech. Symp.*, pp. 579–586, Jan. 2002.

[13] E. J. McCartney, *Optics of the Atmosphere*. Wiley press, 1976.

[14] I. I. Kim, B. McArthur, and E. Korevaar, "Comparison of Laser Beam Propagation at 785 nm and 1550nm in Fog and Haze for Optical Wireless Communications," *Proc. SPIE*, vol. 4214, pp. 26–37, Feb. 2001.

[15] D. Atlas, "Shorter Contribution Optical Extinction by Rainfall," *J. Meterol.*, vol. 10, pp. 486–488, 1953.

[16] H. W. O'Brien, "Visibility and Light Attenuation in Falling Snow," *J. Appl. Meteorol.*, pp. 671–683, 1970.

[17] L. C. Andrews and R. L. Phillips, *Laser Beam Propagation through Random Media*. SPIE press, second ed., 2005.

[18] A. A. Farid and S. Hranilovic, "Optimization of Beam Width, Bit Error Rate and Availability for Free-Space Optical Links," *Proc. IEEE Int. Symp. Commun. Syst. Network Digital Signal Processing*, pp. 92–96, 2008.

[19] E. Korevaar, I. I. Kim, and B. McArthur, "Atmospheric Propagation Characteristics of Highest Importance to Commercial Free Space Optics," *Proc. SPIE*, vol. 4976, pp. 1–12, Apr. 2003.

[20] "Tsunami^{tm} MP.11 Model 5054 Technical Specifications," http://www.proxim.com/products/bwa/multipoint/mp11. [online], last accessed: Mar. 30, 2009.

[21] "IEEE Standard for Local and Metropolitan Area Networks Part 16: Air Interface for Fixed Broadband Wireless Access Systems," 2004. IEEE Std 802.16^{TM}-2004.

[22] "GigaBeam 5.8 Series PtP datasheet," http://www.gigabeam.com/PDFs/GigaBeam5.8PtPdatasheet.pdf. [online], last accessed: Mar. 30, 2009.

[23] "Telsima's Sub-GHz WiMAX(TM) System Demonstrates a 50km (30mile) High Capacity Broadband Internet Connection at 450MHz," http://www.telsima.com/pic/pdf/download/Demo_Brief-50km.pdf. [online], last accessed: Mar. 30, 2009.

[24] R. L. Olsen, D. V. Rogers, and D. B. Hodge, "The aR^b Relation in the Calculation of Rain Attenuation," *IEEE Trans. Antennas Propag.*, vol. AP-26, no. 2, pp. 318–329, Mar. 1978.

[25] D. K. Cheng, *Field And Wave Electromagnaetics*. Addison-Wesley Publishing Company, 1983.

[26] "WiMAX Antenna," http://www.WiMAX-industry.com/ar/10u.htm. [online], last accessed: Mar. 30, 2009.

[27] T. Fujiwara, T. Kasami, and S. Lin, "Error Detecting Capabilities of the Shortened Hamming Codes Adopted for Error Detection in IEEE Standard 802.3," *IEEE Trans. Commun.*, no. 9, pp. 986–989, Sep. 1989.

[28] M. Luby, "LT codes," *Proc. ACM Symp. Found. Comput. Sci.*, pp. 271–280, 2002.

[29] R. Palanki and J. S. Yedidia, "Rateless Codes on Noisy Channels," *Proc. IEEE Int. Symp. Inform. Theory*, p. 38, 2004.

[30] "Virtex-II Pro and Virtex-II Pro X Platform FPGAs: Complete Data Sheet DS083 (v4.7)," www.xilinx.com/support/documentation/data_sheets/ds083.pdf. Xilinx, [online], last accessed: Mar. 30, 2009.
[31] "ISE 9.1 In-Depth Tutorial," http://download.xilinx.com/direct/ise9_tutorials/ise9tut.pdf. Xilinx, [online], last accessed: Mar. 30, 2009.
[32] "XPE Web Power Tools," http://www.origin.xilinx.com/cgi-bin/power-tool/power_virtex2p. Xilinx, [online], last accessed: Mar. 30, 2009.
[33] "DF Raptor Technology Datasheet," http://www.digitalfountain.com/df-raptor-technology-datasheet.html. Digital Fountain, [online], last accessed: Mar. 30, 2009.
[34] "SONAbeam Datasheets," http://www.fsona.com/prod/SONAbeam-Datasheets.pdf. fSONA, [online], last accessed: Mar. 30, 2009.
[35] S. A. Ahson and M. Ilyas, *WiMAX Handbook*. CRC Press, 2007.
[36] "Canada's National Climate Archive," http://www.climate.weatheroffice.ec.gc.ca/. [online], last accessed: Mar. 30, 2009.
[37] S. S. Muhammad, B. Flecker, E. Leitgeb, and M. Gebhart, "Characterization of Fog Attenuation in Terrestrialfree Space Optical Links," *SPIE J. Opt. Eng.*, vol. 46, no. 6, pp. 066001–1–10, Jun. 2007.
[38] "Fog, Canadian Encyclopedia," http://www.thecanadianencyclopedia.com. [online], last accessed: Mar. 30, 2009.

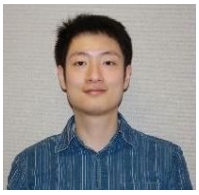

Wenzhe Zhang graduated with a B.Sc degree from Peking University, China in 2007 and with an M.A.Sc. degree from McMaster University, Canada in 2009 both in electrical engineering . He received the ECE Departmental Outstanding Thesis Award for his Master's work. His research work is primarily focused on high-speed wireless communication, channel coding algorithms and encoder/decoder hardware implementation.

Steve Hranilovic (S'94-M'03-SM'07) received the B.A.Sc. degree with honours in electrical engineering from the University of Waterloo, Canada in 1997 and M.A.Sc. and Ph.D. degrees in electrical engineering from the University of Toronto, Canada in 1999 and 2003 respectively.

He is currently an Associate Professor in the Department of Electrical and Computer Engineering, McMaster University, Hamilton, Ontario, Canada. His research interests are in the areas of free-space and wired optical communications, digital communication algorithms, and electronic and photonic implementation of coding and communication algorithms. He is the author of the book *Wireless Optical Communications Systems* (New York:Springer, 2004).

Dr. Hranilovic is a licensed Professional Engineer in the Province of Ontario. In 2006, he was awarded the Government of Ontario *Early Researcher Award*. He is currently the Chair of the joint IEEE Communications/Signal Processing/Information Theory Societies Chapter in the Hamilton Section.

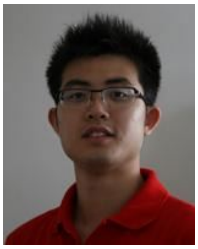

Ce Shi is a forth year undergraduate student in electrical engineering at McMaster University, Hamilton, ON, Canada. From Jan.-Aug. 2008 he worked as an undergraduate research assistant in the Free-Space Optical Communication Algorithms Laboratory. He is currently the Vice President of McMaster Electrical and Computer Engineering Society. His research interests are in mathematical modelling and digital circuit design.